Atmos. Chem. Phys., 17, 13903–13919, 2017
https://doi.org/10.5194/acp-17-13903-2017

Atmospheric Chemistry and Physics
Open Access
EGU

Vegetation greenness and land carbon-flux anomalies associated with climate variations: a focus on the year 2015

Chao Yue[1], Philippe Ciais[1], Ana Bastos[1], Frederic Chevallier[1], Yi Yin[1], Christian Rödenbeck[2], and Taejin Park[3]

[1]Laboratoire des Sciences du Climat et de l'Environnement (LSCE), CEA-CNRS-UVSQ, UMR8212, 91191 Gif-sur-Yvette, France
[2]Max Planck Institute for Biogeochemistry, Jena, Germany
[3]Department of Earth and Environment, Boston University, Boston, MA 02215, USA

Correspondence to: Chao Yue (chao.yue@lsce.ipsl.fr)

Received: 23 December 2016 – Discussion started: 12 January 2017
Revised: 6 September 2017 – Accepted: 10 October 2017 – Published: 23 November 2017

Abstract. Understanding the variations in global land carbon uptake, and their driving mechanisms, is essential if we are to predict future carbon-cycle feedbacks on global environmental changes. Satellite observations of vegetation greenness have shown consistent greening across the globe over the past three decades. Such greening has driven the increasing land carbon sink, especially over the growing season in northern latitudes. On the other hand, interannual variations in land carbon uptake are strongly influenced by El Niño–Southern Oscillation (ENSO) climate variations. Marked reductions in land uptake and strong positive anomalies in the atmospheric CO_2 growth rates occur during El Niño events. Here we use the year 2015 as a natural experiment to examine the possible response of land ecosystems to a combination of vegetation greening and an El Niño event. The year 2015 was the greenest year since 2000 according to satellite observations, but a record atmospheric CO_2 growth rate also occurred due to a weaker than usual land carbon sink. Two atmospheric inversions indicate that the year 2015 had a higher than usual northern land carbon uptake in boreal spring and summer, consistent with the positive greening anomaly and strong warming. This strong uptake was, however, followed by a larger source of CO_2 in the autumn. For the year 2015, enhanced autumn carbon release clearly offset the extra uptake associated with greening during the summer. This finding leads us to speculate that a long-term greening trend may foster more uptakes during the growing season, but no large increase in annual carbon sequestration. For the tropics and Southern Hemisphere, a strong transition towards a large carbon source for the last 3 months of 2015 is discovered, concomitant with El Niño development. This transition of terrestrial tropical CO_2 fluxes between two consecutive seasons is the largest ever found in the inversion records. The strong transition to a carbon source in the tropics with the peak of El Niño is consistent with historical observations, but the detailed mechanisms underlying such an extreme transition remain to be elucidated.

1 Introduction

The first monitoring station for background atmospheric CO_2 concentration was established on Mauna Loa, Hawaii in 1958. Its record shows that atmospheric CO_2 has continued to rise as anthropogenic carbon emissions have increased. However, annual atmospheric CO_2 growth rates (AGR) are lower than those implied by anthropogenic emissions alone, because land ecosystems and the oceans have absorbed part of the emitted CO_2 (Canadell et al., 2007; Le Quéré et al., 2016). On multi-decadal timescales, carbon uptake by land and ocean has kept pace with growing carbon emissions (Ballantyne et al., 2012; Li et al., 2016), exerting a strong negative feedback to global change. Over land, increasing carbon uptake is consistent with worldwide vegetation greening as revealed by satellite observations (Zhu et al., 2016). Long-term warming and CO_2 fertilization have contributed to growing-season greening and increasing land carbon uptake in northern latitudes, which further leads to a markedly increasing seasonal atmospheric CO_2 amplitude (Forkel et al., 2016; Graven et al., 2013; Myneni et al., 1997). At the

same time, large year-to-year fluctuations occur in the terrestrial carbon sink especially over tropical lands. These fluctuations mainly occur in response to climate variations induced by the El Niño–Southern Oscillation (ENSO; Wang et al., 2013, 2014) and other occasional events such as volcanic eruptions (Gu et al., 2003). The occurrence of El Niño events often leads to elevated temperatures with reductions in precipitation over tropical lands; these cause sustained droughts that substantially reduce the land carbon uptake (Doughty et al., 2015). These ENSO-associated tropical land uptake variations have translated into large variations in atmospheric CO_2 growth rates, which are found to be significantly correlated with tropical land temperature anomalies (Wang et al., 2014).

Understanding such driving mechanisms and variations in land carbon uptake is essential if we are to predict future carbon-cycle feedbacks on global environmental changes – including climate change. Growing-season normalized difference vegetation index (NDVI) observed by the moderate-resolution imaging spectroradiometer (MODIS) aboard the Terra satellite has consistently increased since 2000 over northern latitudes (Bastos et al., 2017). The positive link between seasonal NDVI and vegetation photosynthesis is well established for deciduous forests in temperate and boreal biomes (Gamon et al., 1995), and NDVI is often assumed as a surrogate for vegetation growth. Nevertheless, it is unclear whether, on an annual timescale, higher NDVI anomalies are indeed always associated with higher carbon-uptake anomalies. A few studies have reported important seasonal coupling in vegetation greenness and land carbon uptake in mid- to high latitudes, with summer drought likely compensating for enhanced spring uptake (Angert et al., 2005; Wolf et al., 2016). While spring warming may enhance vegetation growth and carbon uptake, autumn warming can lead to net carbon loss by enhancing respiration carbon loss (Piao et al., 2008). Furthermore, greening and browning may occur in different regions within the same growing season (Bastos et al., 2017), so that the associated consequence on land carbon dynamics needs to be investigated. Such an investigation on the relationship between seasonal NDVI dynamics and land carbon uptake will help to predict future land carbon sink capacity.

El Niño events are often linked to enhanced drought conditions in Amazonian forest with widespread increases in tree mortality and drops in ecosystem carbon storage (Phillips et al., 2009). Fire emissions from Asian tropical regions also show a nonlinear increase with drought during El Niño, another factor that reduces land carbon sequestration (Field et al., 2016; Yin et al., 2016). With future anthropogenic climate change, it is projected that the frequency of extreme El Niño events will be doubled (Cai et al., 2014). It is not clear how future carbon dynamics will respond to such a doubling of extreme El Niño events, or whether any extreme phenomena in the carbon cycle might occur as a consequence. The year of 2015 is a good test case for investigating El Niño-related phenomena because it contained the strongest El Niño event since the one in 1997–1998 and occurred at a time when unprecedented mean annual land temperature was observed.

We use the year 2015 as a natural experiment to investigate the response of land ecosystems to a combination of extreme greening and an El Niño event. The year 2015 had the greenest growing season in the Northern Hemisphere since 2000, in particular over eastern North America and large parts of Siberia (Bastos et al., 2017), and this was accompanied by the highest mean annual global land temperature on record since 1880 (https://www.ncdc.noaa.gov/cag/time-series/global/globe/land/ytd/12/1880-2015). At the same time, a strong El Niño event developed starting in the latter half of 2015. Elevated fire emissions in tropical Asia were reported (Huijnen et al., 2016; Yin et al., 2016) and a severe drought was detected over eastern Amazonia (Jiménez-Muñoz et al., 2016). As a result, in 2015 the global monthly atmospheric CO_2 concentration surpassed 400 $\mu mol\,mol^{-1}$ (ppm) for the first time, with an unprecedented large annual growth rate of $2.96 \pm 0.09\,ppm\,yr^{-1}$ (https://www.esrl.noaa.gov/gmd/ccgg/trends/global.html#global_growth). We examined global and regional land–atmosphere carbon fluxes estimated from two atmospheric inversions for 1981–2015. Seasonal patterns in the land carbon uptake in 2015 relative to the long-term trend of 1981–2015 were examined and linked to extreme climate anomalies. To put the 2015 land response into a historical context, we also examined the relationship between historical land carbon-uptake anomalies, and NDVI and climate anomalies, in order to infer general patterns in factors driving the land carbon-uptake anomalies. Our findings are expected to provide insights into future land carbon-cycle feedbacks to vegetation greening and climate variations.

2 Data and methods

2.1 Data sets

2.1.1 Atmospheric inversion data

We used two gridded land and ocean carbon-uptake data sets based on atmospheric CO_2 observations, namely those from the Copernicus Atmosphere Monitoring Service (CAMS) inversion system developed at the LSCE (Chevallier et al., 2005, 2010) and the Jena CarboScope inversion system developed at the MPI for Biogeochemistry, Jena (update of Rödenbeck, 2005; Rödenbeck et al., 2003). Atmospheric inversions estimate land– and ocean–atmosphere net carbon fluxes by minimizing a Bayesian cost function, accounting for the mismatch between the observed and simulated atmospheric CO_2 mixing ratios. To do this, they use atmospheric CO_2 concentrations at measurement sites, combined with an atmospheric transport model and prior information on fos-

sil fuel carbon emissions and carbon exchange between the atmosphere and land (and ocean). Detailed information on these two atmospheric inversions can be found in the references above.

The CAMS inversion data (version r15v3) were provided for 1979–2015 with a weekly time step and a spatial resolution of 1.875° latitude and 3.75° longitude. The Jena CarboScope inversion provides daily fluxes at a spatial resolution of 3.75° latitude and 5° longitude and offers a series of runs. All runs provide data covering the whole period of 1979–2015, but they have different validity periods that focus on using different sets of CO_2 measurement stations. Within the validity period, all employed stations have valid CO_2 observations, i.e. they have coherent and complete measurements over time. The idea of a validity period is to avoid spurious flux variations resulting from a changing station network. It is optimal to examine temporal trends within the validity period, but this does not mean the data outside this period are invalid and should be discarded. From the Jena inversion runs, we selected s04_v3.8 (shortened as Jena04 in the main text and the Supplement). Jena04 used the largest number of measurement sites for 2015 and therefore had the most detailed constraint on carbon exchanges for this year (see http://www.bgc-jena.mpg.de/CarboScope/ for more details on other configurations). The validity period of the Jena04 data is 2004–2015, but here we used the data available for the whole time span of 1981–2015. This is necessary to provide both the large number of sites in 2015 and the long historical period, which is needed to produce a robust anomaly estimate. We compared the linear trends obtained over large latitudinal regions between the Jena04 run and the long s81_v3.8 run (the latter has a validity period of 1981–2015 but far fewer sites are included than in Jena04), and confirmed that the derived trends are similar. The same issue of evolving site number and data coverage with time also occurs for the CAMS inversion, but the CAMS inversion uses sites with at least a 5-year run of data. CAMS therefore has a denser (during the recent decade) but temporally evolving data coverage than CarboScope.

Estimates of land and ocean net carbon uptakes for 1981–2015 from the Global Carbon Project (GCP; Le Quéré et al., 2016) were compared with the inversion data. For this purpose, an annual global carbon flux of $0.45\,\mathrm{Pg\,C\,yr^{-1}}$ is subtracted from the inversion-derived land carbon uptakes and is added to ocean carbon uptakes to account for the preindustrial land-to-ocean carbon fluxes induced by river transport (Jacobson et al., 2007), following Le Quéré et al. (2016). Ocean carbon uptakes in the GCP estimates are based on the mean CO_2 sink estimated for the 1990s from observations, and the trend and variability in the ocean CO_2 sink for 1959–2015 from global ocean biogeochemistry models. Estimates of land carbon uptake in the GCP estimates are calculated as the difference between anthropogenic emissions, atmospheric CO_2 growth and the ocean sink. In summary, the estimates of land and ocean carbon uptake in the GCP estimates are largely independent from the two inversions used here, except that the CO_2 records from atmospheric stations that are used in the inversions are also used in the GCP estimates.

2.1.2 Atmospheric CO_2 growth rates, NDVI and climate data

Atmospheric CO_2 growth rates were retrieved from the Global Monitoring Division, Earth System Research Laboratory (ESRL), NOAA (http://www.esrl.noaa.gov/gmd/ccgg/trends/global.html). We used NDVI data between 2000 and 2015 from MODIS Terra Collection 6 (Didan, 2015), at a resolution of 0.05° and a 16-day time step. NDVI data are processed from MODIS land surface reflectance data and thoroughly corrected for atmospheric effects. We were strict in applying quality assurance controls to maintain a distinct seasonal trajectory of vegetative radiometric observations and minimize spurious signals (e.g. snow or cloud). Detected unexpected non-vegetative observations were first excluded and then filled using the adaptive Savitzky–Golay filter (Chen et al., 2004; Jönsson and Eklundh, 2004). The Savitzky–Golay filter is a simplified convolution over a set of consecutive values with weighting coefficients given by a polynomial least squares fit within the filter window (Savitzky and Golay, 1964). After this procedure, the linearly interpolated daily NDVI data were used to calculate mean seasonal NDVI and regridded at 0.5° resolution, with pixels of seasonal NDVI lower than 0.1 being further masked to ensure robustness. We examined four seasons: Q1 (January–March), Q2 (April–June), Q3 (July–September) and Q4 (October–December). Climate fields are from the ERA-Interim reanalysis (Dee et al., 2011) at 0.5° resolution and monthly time step. We used air temperature, precipitation and volumetric soil water content (%) integrated over the soil column to a depth of 2.89 m.

2.1.3 Indices for El Niño–Southern Oscillation (ENSO) states and fire emission data

We examined the seasonal variations of the carbon cycle in 2015 in relation to ENSO events and compared the 2015 El Niño event with that of 1997–1998. The Multivariate ENSO Index (MEI, http://www.esrl.noaa.gov/psd/enso/mei/; Wolter and Timlin, 2011) was used to indicate the ENSO state. MEI is a composite index calculated as the first unrotated principal component of six ENSO-relevant variables (including sea level pressure and sea-surface temperature) over the tropical Pacific for each of 12 sliding two-monthly seasons. MEI has been widely used in previous studies of land carbon dynamics as an indicator of ENSO states (Nemani et al., 2003; van der Werf et al., 2008). The 12 two-monthly MEI values for each year are summed to obtain the annual MEI. The interannual variations in climate and land carbon uptake are linked with MEI to infer a general relationship between land carbon dynamics and ENSO climate oscillations. To examine the po-

tential role of fire emissions in the land carbon balance in 2015, we used the Global Fire Emissions Database version 4s (GFED4s) carbon emission data at daily time step and 0.25° spatial resolution (http://www.globalfiredata.org/data.html). Monthly fire-carbon emissions were calculated for the regions and were examined for 1997–2015.

2.2 Data analysis

2.2.1 NDVI rank analysis and greening trend

We first examine the vegetation greenness status in the year 2015. Given a season and a pixel, the annual time series of seasonal NDVI for 2000–2015 were ranked in ascending order so that each year could be labelled by a rank, with 1 being the lowest and 16 being the highest. A spatial map of NDVI rank was then obtained for each year for the given season (Fig. S1 in the Supplement). A composite map was made for 2015, by merging pixels with the highest rank of all four seasons in 2015 (Fig. 1a). Vegetated area fraction with the highest rank for different years was obtained, with the sum of these fractions yielding unity. This procedure was repeated for all four seasons to generate four seasonal time series, with each time series containing the vegetation land fractions with highest NDVI for different years (Fig. 1b). Note that NDVI values for the Northern Hemisphere for Q1 and Q4 mostly fall outside the growing season (although October is frequently considered within the growing season and some evergreen coniferous forests show significant photosynthetic activities in March in regions with mild winters, e.g. Tanja et al., 2003), so that a valid NDVI might not necessarily be associated with significant seasonal vegetation activity. However, we expect that this issue will be partly alleviated by our applied rigorous quality assurance control in preprocessing and a minimum threshold of 0.1 on seasonal NDVI. Such seasonal segregation is adopted mainly because of its general applicability across the globe, especially for tropical ecosystems where seasonality in vegetation activities is minimal.

2.2.2 Analysis of land carbon-uptake dynamics associated with climate variations

Annual land and ocean carbon uptake and carbon emissions from the two inversions were calculated for the globe over their period of overlap, 1981–2015. AGRs from NOAA/ESRL for 1981–2015 were converted into Pg C units using a conversion factor of 2.12 Pg C ppm^{-1} (Ballantyne et al., 2012; Prather et al., 2012; Le Quéré et al., 2016), in order to examine the closure of the global carbon balance in the inversion data. The conversion factor used here assumes that the entire atmosphere is well mixed over 1 year. We disaggregated the record high AGR in 2015 into individual components of emissions and sinks. The record high AGR in 2015 was a composite effect collectively determined by carbon emissions from fossil fuel burning and industry, and land and ocean carbon uptakes. All of these were impacted by an historical trend (Fig. 2). Therefore, to understand the factors contributing to 2015's record AGR, we separated it into a long-term trend and interannual anomalies. Annual time series of carbon emissions, land and ocean carbon uptakes, and AGRs from NOAA/ESRL for 1981–2015 were linearly detrended. The percentages of anomalies in carbon emissions, land and ocean sinks in 2015 to the 2015 AGR anomaly, were then calculated as relative contributions by each factor to the 2015 AGR anomaly.

Seasonal land carbon-uptake anomaly time series were also calculated by subtracting the same linear trend for 1981–2015. The globe was divided into three latitude bands: boreal Northern Hemisphere (BoNH, latitude > 45° N), temperate Northern Hemisphere (TeNH, 23.5° N < latitude < 45° N), and tropics and extratropical Southern Hemisphere (TroSH, latitude < 23.5° N). The BoNH and TeNH are grouped as boreal and temperate Northern Hemisphere (BoTeNH, latitude > 23.5° N) when examining seasonal carbon transitions. Seasonal land carbon-uptake anomalies were then calculated for each region and the whole globe, with positive anomalies indicating enhanced sink (or reduced source) against the linear trend (i.e. the normal state), and negative ones indicating the opposite. The same seasonal linear detrending was also performed for climate fields of air temperature, precipitation and soil water content. The relationship between anomalies in land carbon uptake, and temperature and precipitation is examined using partial correlation coefficients in a multivariate linear regression framework with an ordinary least squares method. The relationships between seasonal land carbon-uptake anomalies and NDVI anomalies were also examined using a simple linear regression.

We then especially examined the seasonal anomalies of land carbon uptake in 2015 and the carbon-uptake transitions between two consecutive seasons, to reveal any extreme phenomena in the land carbon cycle that might lead to the abnormally high AGR in 2015. Seasonal land carbon-uptake transitions are calculated as the land sink anomaly in a given season minus that of the previous one. When examining transitions of land carbon-uptake anomalies by the CAMS inversion, we found that the year 1993 had an extremely negative Q3→Q4 global transition (−2.85 Pg C within 6 months, $< -4\sigma$, the second lowest being the year 2015 with −1.0 Pg C) albeit with a reasonable annual land carbon uptake (3.75 Pg C yr^{-1}). This is linked to an extreme high Q3 and low Q4 uptake in this year, which could not be explained by any known carbon-cycle mechanisms. This is thus identified as a result of numerical instability of the inversion system for that release and consequently the year 1993 has been removed from all of the aforementioned seasonal analyses. However, we identified that the temporal trends for annual and seasonal land carbon uptakes show almost no change whether including or not including the year 1993.

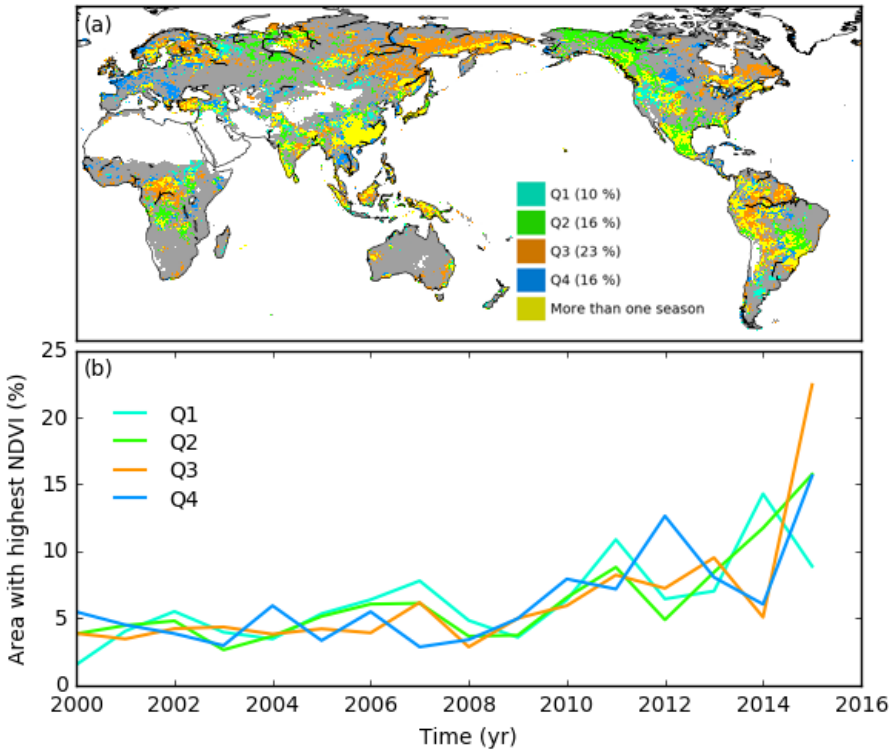

Figure 1. Year 2015 as the greenest year for the period 2000–2015. **(a)** Distribution of seasons for which 2015 NDVI ranks the highest during the period 2000–2015. Yellow-coloured pixels indicate grid cells where 2015 NDVI ranks highest for more than one season. For each season, the fraction of global vegetated land area for which 2015 NDVI ranks highest is shown in the coloured legend. **(b)** Temporal evolution of the percentage of vegetated land with highest NDVI for 2000–2015 for each season and different years. The sum total of vertical-axis values for each season over all years is 100 %. Q1 is January–March, Q2 is April–June, Q3 is July–September and Q4 is October–December.

3 Results

3.1 Vegetation greening in 2015

Figure 1a illustrates where and when higher-than-normal greening conditions were observed in different seasons of the year 2015, compared to other years of 2000–2015 (see Fig. S1 for the greenness distribution of each season). On average over the four seasons of 2015, 16 % of vegetated land shows record seasonal NDVI. The year with the second highest NDVI is 2014 with 9 % vegetated area having record high NDVI. An increase in the record-breaking NDVI occurrence over time is clearly seen in Fig. 1b. In short, 2015 clearly stands out as a greening outlier, having the highest proportion of vegetated land being the greenest for all four seasons except for the first season (despite the fact that for Q1, 2015 is still the third highest; Q1 is January–March).

For boreal and temperate regions of the Northern Hemisphere, the seasons with highest NDVI in 2015 are dominated by Q2 and Q3 (Q2 is April–June; Q3 is July–September), corresponding to the growing season from spring to early autumn (Fig. S2). A pronounced greening anomaly in Q2 occurred in western to central Siberia, western Canada and Alaska, and eastern and southern Asia (Fig. S1). Central and eastern Siberia and eastern North America showed marked greening in Q3. Strong and widespread greening also occurred in the tropics during Q3 across Amazonia and the savanna (or cerrado) of eastern South America and tropical Africa, but this strong positive greening signal greatly diminished in Q4 (Q4 is October–December) especially in central to eastern Amazonia with the development of El Niño (Fig. S1). Overall, the strongest greening in 2015 across the globe is dominated by northern lands (latitude > 23.5° N), while for the northern tropics (0–23.5° N) only moderately strong greening is found, and for the Southern Hemisphere the greening of 2015 is close to the average state for the period of 2000–2015 (Fig. S3). The extreme growing-season greening in northern lands is confirmed as being a robust result by Bastos et al. (2017), who used Terra MODIS NDVI data with different quality control procedures, and consistency is also confirmed between Terra and Aqua sensors (Fig. S1 in Bastos et al., 2017).

3.2 Global carbon balance for 1981–2015

Figure 2 shows (a) the time series of fossil fuel burning and industrial carbon emissions, (b) NOAA/ESRL AGRs linked

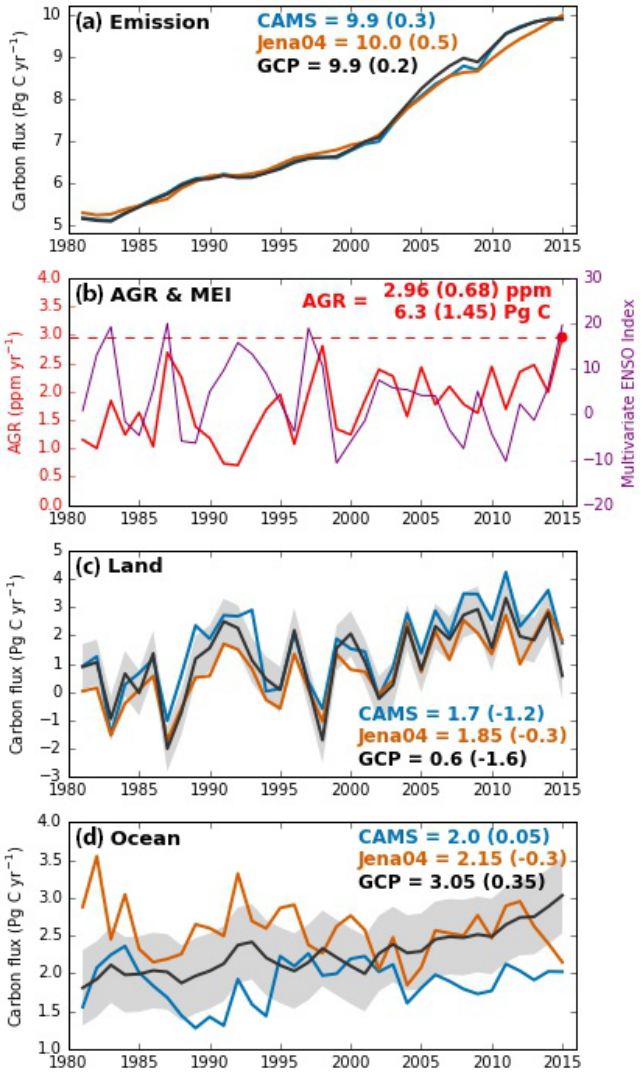

Figure 2. Global carbon fluxes and atmospheric CO_2 growth rates for 1981–2015. **(a)** Carbon emissions from fossil fuel and industry used in the CAMS (blue) and Jena04 (orange) inversions, **(b)** annual atmospheric CO_2 growth rate (AGR, in red) from NOAA/ESRL linked to Multivariate ENSO Index (MEI, in purple), **(c)** land and **(d)** ocean carbon sinks for 1981–2015. Emissions, land and ocean carbon sinks from the Global Carbon Project (GCP, in black) are also shown for comparison. In panels **(c)** and **(d)**, a carbon flux of 0.45 Pg C yr^{-1} was used to correct inversion-derived land and ocean sinks to account for preindustrial land-to-ocean carbon flux as in Le Quéré et al. (2016). All numbers indicate values in 2015 (Pg C yr^{-1}, rounded to ± 0.05 Pg C yr^{-1}), with those in brackets showing linearly detrended anomalies for the same year.

to ENSO climate oscillations as indicated by the MEI, and (c and d) land and ocean carbon sinks for the common period of the two inversions (1981–2015), with the estimates by the GCP. Emissions show a clear increase with time but AGRs are more variable. The record high AGR of 2.96 ppm in 2015 exceeds those in all previous years including the extreme El Niño event in 1997–1998, despite much higher annual emissions in 2015. Interannual variability in AGR is mainly caused by fluctuations in the land carbon sink, with Pearson's correlation coefficients between detrended AGR and land sink less than -0.8 ($p < 0.01$) for both inversions (Pearson's correlation coefficient between detrended AGR and MEI being 0.27, $p < 0.1$). The root mean square differences between inversion and GCP carbon sinks are 0.70 and 0.65 Pg C yr^{-1} for CAMS and Jena04, respectively, for the land, and ~ 0.5 Pg C yr^{-1} for the ocean for both inversions. These are within the uncertainties of 0.8 and 0.5 Pg C yr^{-1} for 1981–2015 for land and ocean, respectively, as reported by the GCP. The interannual variability of detrended sink anomalies for the land agrees well between the inversions and the GCP estimates (with Pearson's correlation coefficients being 0.9 for both inversions, $p < 0.01$).

For 2015, the prescribed anthropogenic carbon emissions in the CAMS inversion are 9.9 Pg C yr^{-1}, of which 2.0 Pg C are absorbed by ocean, 1.7 Pg C by land ecosystems, and 6.2 Pg C remaining in the atmosphere, which matches the AGR from background stations of 6.3 Pg C assuming a conversion factor of 2.12 Pg C ppm^{-1} (Ballantyne et al., 2012; Le Quéré et al., 2016) and considering a measurement uncertainty in AGR of 0.09 ppm (0.2 Pg C) for 2015. When land carbon fluxes from the inversion are linearly detrended for 1981–2015, the terrestrial sink in 2015 is 1.2 Pg C lower than normal (i.e. the trend value), but this is not an extreme value – it is only the seventh weakest sink since 1981. This weaker land carbon-uptake accounts for 82 % of the positive AGR anomaly, which is 1.45 Pg C in 2015 by subtracting a linear temporal trend. Jena04 yields an AGR in 2015 that is 0.13 ppm lower than the AGR based on background stations only, a difference close to the observation uncertainty. After removing the linear trends over time similarly as for the CAMS inversion, the land carbon-uptake anomaly for Jena04 is -0.3 Pg C yr^{-1} in 2015, or 20 % of the observed AGR anomaly, the remaining being explained by a positive anomaly in fossil fuel emissions (34 %), a negative anomaly in the ocean sink (20 %), and the difference between modelled AGR and NOAA/ESRL reported AGR. Note that the land sink given by the GCP data for 2015 is much lower than in the two inversions, with a detrended anomaly lower than that of CAMS, indicating an even larger contribution from land to the high anomaly of AGR.

In general, the warm phases of ENSO events are associated with positive anomalies in land air temperature, negative precipitation anomalies and lower land carbon-uptake anomalies (Fig. 3); this is consistent with previous studies (Cox et al., 2013; Wang et al., 2014). The lower precipitation during El Niño is due to a shift of precipitation from tropical land to the ocean (Adler et al., 2003), and higher land temperature might be due to reduced evaporative cooling. The two extreme El Niño years of 1997 and 2015 have rather close MEI values. Compared with the "standard" El Niño state of temperature and precipitation represented by the regression line, the year

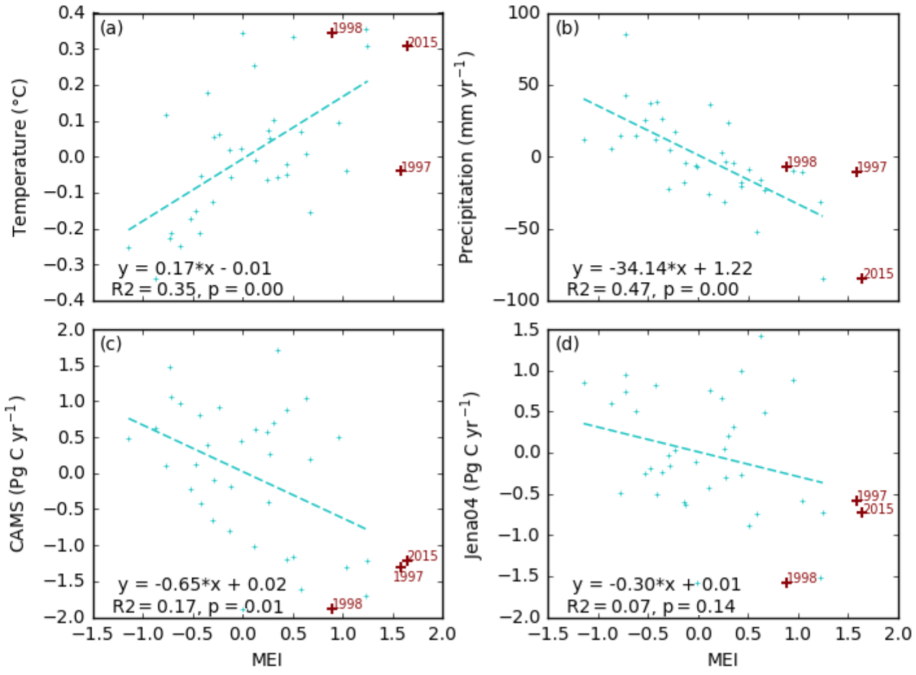

Figure 3. Relationships between anomalies of **(a)** land air temperature, **(b)** land precipitation, **(c)** land carbon fluxes by the CAMS inversion, **(d)** land carbon fluxes by the Jena04 inversion and the Multivariate ENSO Index (MEI). All variables are linearly detrended for 1981–2015.

1997 was relatively "cool" and "wet", while 2015 was rather "warm" and "dry" (with an extremely negative precipitation anomaly). Year 1998 has a smaller value of MEI than 1997 or 2015, but has a higher temperature anomaly than 2015, and a much lower land carbon-uptake anomaly than 1997 and 2015 in both inversions, while the land carbon-uptake anomalies in 1997 and 2015 are similar. A more detailed comparison of these 3 years and their carbon-cycle dynamics will be presented in the Discussion section.

3.3 Seasonal land carbon-uptake dynamics associated with climate variations with a focus on 2015

Figure 4 shows the partial correlation coefficients between anomalies in seasonal land carbon uptake and those in seasonal temperature and precipitation for different regions. The simple, individual (univariate) linear relationships between detrended anomalies in land carbon fluxes and those in temperature and precipitation are presented in the Supplement (Figs. S4 and S5). Land carbon fluxes show consistent relationships with temperature between the two inversions for BoNH: a positive relationship for Q2 and a negative one for the other three seasons (with Q1 by Jena04 being the only one with a non-significant correlation). Partial correlations between land carbon fluxes and precipitation are absent or non-significant for BoNH. This points to the fact that vegetation productivity in BoNH is in principle dominated by temperature, with warmer spring and early summer (Q2 is April–June) enhancing vegetation net carbon uptake, but a higher temperature in later summer, autumn and early winter reducing the land capacity to sequester carbon, consistent with previous studies (Piao et al., 2008). For TeNH, a significant negative relationship is found between land fluxes by the CAMS inversion and temperature for Q3, and both inversions show negative relationships between land fluxes and precipitation for Q4, probably due to enhanced early autumn respiration under wetter conditions. For TroSH, land carbon uptakes in Q1, Q2 and Q4 are all negatively related to temperature ($p < 0.05$ for both inversions), while an increase in precipitation in Q1 is found to be associated with enhanced land carbon uptake.

To explain the apparent paradox in 2015 between the strong greening and an only moderate terrestrial uptake, we examined in detail the seasonal land carbon-flux anomalies in 2015 (Fig. 5; refer to Fig. S6 for the spatial distribution of flux anomalies). On a seasonal scale, both inversions indicate positive carbon-uptake anomalies during Q2 and Q3 for BoTeNH (latitude > 23.5° N), consistent with marked greening in central to eastern Siberia, eastern Europe and Canada (Fig. 1) as outlined above. Indeed, both BoNH and TeNH show positive relationships between seasonal land carbon-flux anomalies and NDVI anomalies for Q2 and Q3, with BoNH showing moderate greenness (after a linear trend is removed) for Q3, and TeNH showing extreme greenness for Q2 in 2015 (Fig. S7). However, an extreme follow-up negative (source) anomaly occurred in Q4 (Fig. 5a). These negative anomalies were lower than the 10th percentile of all anomalies in Q4 over time for both inversions and they partly

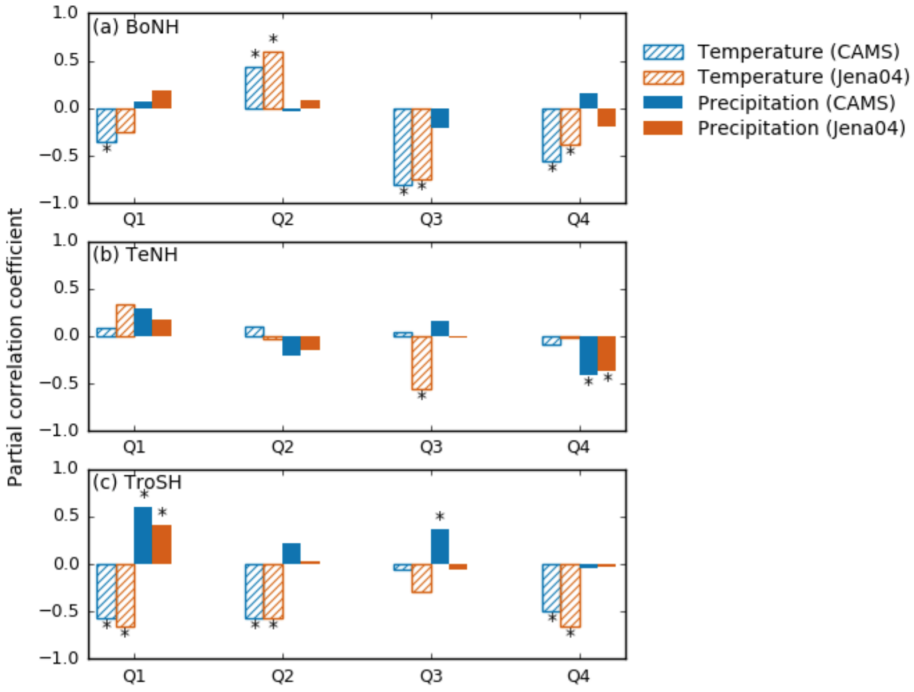

Figure 4. Partial correlation coefficients of detrended annual anomalies of land carbon fluxes by CAMS and Jena04 inversions against the anomalies in temperature and precipitation of different seasons ($n = 34$). An asterisk indicates significant correlation ($p < 0.05$).

cancelled the extra uptake in Q2 and Q3. As a result, on an annual timescale, the CAMS inversion shows an almost neutral land flux anomaly in BoTeNH, while the Jena04 inversion still indicates a significant positive annual anomaly.

For the tropics and extratropical Southern Hemisphere (TroSH, latitude < 23.5° N), both inversions show a weak negative land carbon anomaly for Q1 (mean value of −0.10 Pg C) in 2015, moderate anomalies in Q2 (of differing signs, with a negative one of −0.3 Pg C in CAMS and a positive one of 0.2 Pg C in Jena04). Q3 anomalies are almost carbon neutral for both inversions. In stark contrast, between Q3 and Q4, both inversions show a strong shift towards an abnormally large land carbon source (i.e. negative anomalies of ∼ −0.7 Pg C against a carbon source expected from the linear trend, lower than the 10th percentile over time in both inversions). On an annual timescale, CAMS shows a large negative anomaly of −1.2 Pg C. For Jena04, sink and source effects in Q1–Q3 cancelled each other, leaving the annual anomaly the same as in Q4.

Over the globe, the Jena04 inversion shows an abnormally strong sink during Q2 (normal state being a net carbon sink), owing to the synergy of enhanced Q2 uptakes in both BoTeNH and TroSH. This abnormally enhanced uptake partly counteracted the strong shift towards a source in Q4 (normal state being a net carbon source), leaving a small negative annual land carbon balance of −0.3 Pg C. For the CAMS inversion, because of the co-occurrence of enhanced carbon release in BoTeNH and the sudden shift towards a large carbon source in TroSH both in Q4 (normal state for both being a net carbon source), the land shows a strong global shift towards being a source in Q4, leaving a negative annual carbon anomaly of −1.2 Pg C (i.e. carbon sink being reduced compared with the normal state).

These consistent results from both inversions point to very strong seasonal shifts in the land carbon balance as an emerging feature of 2015. We thus calculated *transitions* in land carbon-uptake anomaly as the difference in flux anomalies between two consecutive seasons (defined as the anomaly in a given season minus that in the previous one) for all years of the period 1982–2015 (Fig. 6). The ranks of transitions for different seasons relative to other years between the two inversions are broadly similar, except for Q1 → Q2 and Q2 → Q3 in TroSH, mainly due to the differences between the two inversions in seasonal land carbon-uptake anomaly in Q2 (Fig. 5b). On the global scale, both inversions show an extreme transition to a negative uptake anomaly for Q3 → Q4, with 2015 being the largest transition of the period 1982–2015 (a transition towards an enhanced carbon source of −1.0 Pg C in 6 months). The abnormal transitions for Q3 → Q4 on the global scale are located in the TroSH region, where both inversions show that during 1982–2015 the largest transition occurred in 2015. For BoTeNH, both inversions showed strong transitions towards positive anomaly for Q1 → Q2; however, the same strong transition towards source anomaly occurred in Q3 → Q4, partly cancelling the sink effects during growing seasons.

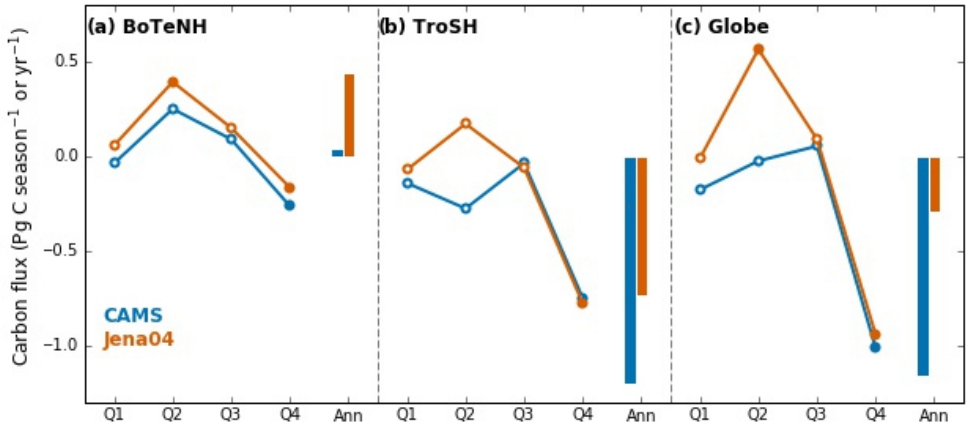

Figure 5. Seasonal land carbon-uptake anomalies in 2015. Data are linearly detrended for 1981–2015 for different seasons in 2015, by CAMS (blue) and Jena04 (orange) inversion data. Open or solid dots indicate seasonal values (Pg C season^{-1}) and vertical bars indicate annual sums (Pg C yr^{-1}). Data are shown for: **(a)** boreal and temperate Northern Hemisphere (BoTeNH, > 23.5° N), **(b)** tropics and extratropical Southern Hemisphere (TroSH, < 23.5° N) and **(c)** the whole globe. Solid dots indicate seasonal land carbon-uptake anomalies below the 10th or above the 90th percentiles for 1981-2015.

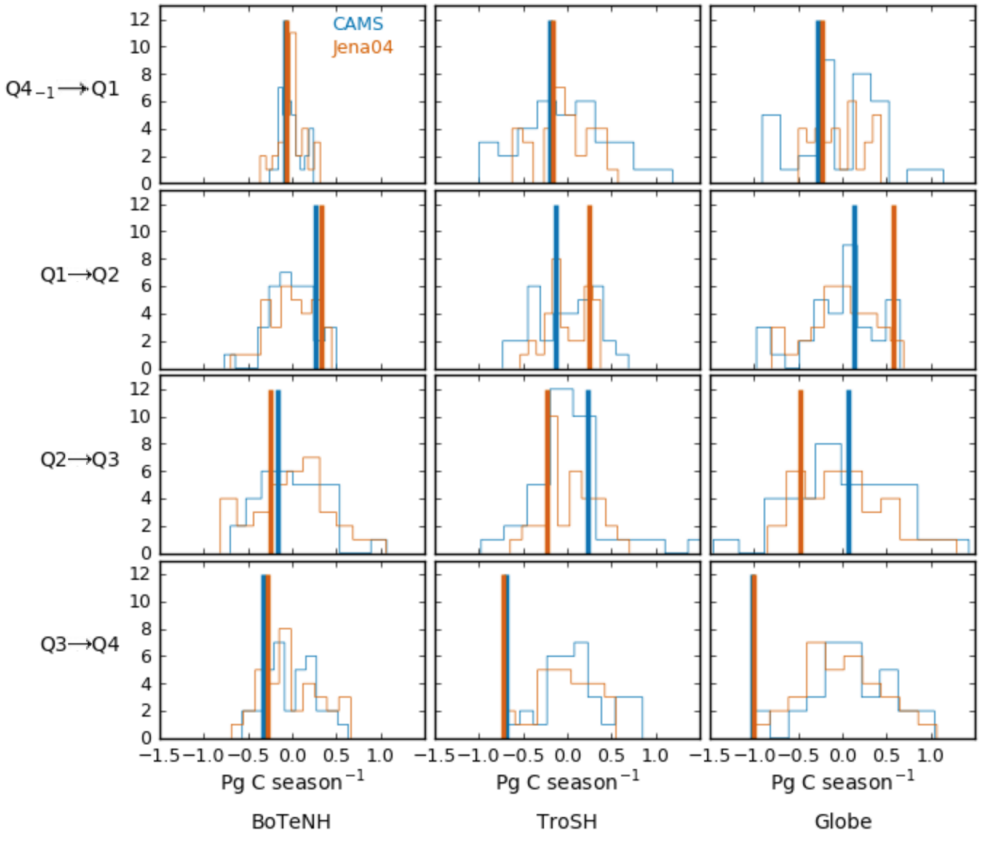

Figure 6. Extremeness of transitions in seasonal land carbon-uptake anomaly in 2015. Lines of histograms for seasonal land carbon-uptake transitions for 1981–2015 are shown for boreal and temperate Northern Hemisphere (BoTeNH, latitude > 23.5° N), tropics and extratropical Southern Hemisphere (TroSH, latitude < 23.5° N) and the whole globe. A transition between two consecutive seasons is defined as the linearly detrended land carbon-uptake anomaly in a given season minus that in the former one. The horizontal-axis shows the seasonal transitions in land carbon-uptake anomalies (Pg C season^{-1}). Vertical orange solid lines indicate values for 2015.

4 Discussion

4.1 Land carbon-uptake dynamics with climate variations in northern latitudes and seasonal transitions of land carbon uptake in 2015

The two inversions consistently allocate a strong positive carbon-uptake anomaly in the region of BoTeNH during spring, which persists through the summer (Q2–Q3): an extreme sink anomaly is estimated in Q2 by Jena04, but a more moderate one by CAMS (still above the 75th percentile). The strong sinks in Q2 in both inversions are dominated by TeNH regions (23.5° N < latitude < 45° N; Fig. S8). For this region, both inversions show a strong positive correlation between carbon-uptake anomalies and NDVI in Q2, with an extremely high NDVI anomaly in 2015 (Fig. S7f). Thus, the strong sinks in Q2 are evidently linked to the extreme greening, while temperature and precipitation anomalies were only moderate (Figs. S4f and S5f).

For Q3, an extreme carbon sink anomaly occurs in BoNH (latitude > 45° N) in CAMS; however, an equally strong negative anomaly (i.e. reduced sink) was found in TeNH in the same season, leaving the whole BoTeNH region only a moderately positive sink anomaly (Fig. S8). For TeNH alone, CAMS indicates an extreme seasonal shift from a positive anomaly in Q2 to a negative one in Q3. This implies strong seasonal transitions resulting from enhanced ecosystem CO_2 release after growing-season uptake and the presence of seasonal coupling in land carbon dynamics. For TeNH in 2015, NDVI persisted from a high extreme in Q2 to close to normal in Q3 (Fig. S7f, g), and temperature remained moderate for both Q2 and Q3 (Fig. S4f, g), but precipitation shifted from a moderate anomaly in Q2 to an extremely low one (Fig. S5f, g). In summary, the shift from a strong Q2 sink anomaly to a strong Q3 source anomaly by CAMS might be linked to the shift in precipitation and drought in Q3, such as the prevailing drought in Europe as shown in Fig. S9 (see also a detailed discussion of the European drought by Orth et al., 2016).

The Jena04 inversion agrees with a higher-than-normal sink in TeNH (23.5° N < latitude < 45° N) during spring (Q2). It also reports a moderate positive anomaly for Q3 in BoNH, but does not show a strong negative anomaly (i.e. reduced sink) in TeNH in Q3 as CAMS does (Fig. S8). This is possibly related to differences in the measurement station data used, to different land prior fluxes (from the ORCHIDEE model in CAMS, and the LPJ model in Jena CarboScope), or to the fact that the Jena04 inversion has a larger a priori spatial error correlation length for its land fluxes (1275 km) than CAMS (500 km) (Chevallier et al., 2010; Rödenbeck et al., 2003). Nonetheless, both inversions consistently indicate that the enhancement of CO_2 uptake during spring and summer on the northern hemispheric scale was subsequently offset by an extreme source anomaly in autumn (Q4).

The large carbon source anomalies in Q4 shown by the two inversions in BoTeNH seem to be dominated by different factors in BoNH versus TeNH. In BoNH the source anomaly in 2015 is more linked to elevated temperature in Q4, which shows a significant negative correlation with carbon-uptake anomalies by both inversions (Fig. S4d). In contrast, precipitation in Q4 has no correlation with carbon-uptake anomalies, and precipitation in 2015 was close to the normal state (Fig. S5d). The prevailing high temperature in Q4 of 2015 is especially evident over most of north America, central to eastern Siberia and Europe (Fig. S9a).

In TeNH, the roles of temperature and precipitation are reversed compared to BoNH. Q4 precipitation is found to have a significant negative correlation with land carbon-uptake anomalies for both inversions, and Q4 in 2015 was characterized by a very high precipitation anomaly, leading to a reduced land carbon uptake (Fig. S5h). While temperature in Q4 of 2015 was moderately high, no significant correlation is found between carbon-uptake anomalies and temperature (Fig. S4h). However, for both BoNH and TeNH, NDVI remained moderately high in Q4 of 2015 (Fig. S7d, h).

The positive relationship between land carbon uptake and temperature in Q2 (spring and early summer), and a negative one for Q3 and Q4 (autumn) for BoNH, are in line with previous studies. Several studies reported an enhanced greening during spring and summer in the Northern Hemisphere (Myneni et al., 1997; Zhou et al., 2001), as driven by increasing spring and summer temperatures (Barichivich et al., 2013; Nemani et al., 2003), leading to enhanced land carbon uptake and a long-term increase in the seasonal amplitude of atmospheric CO_2 in northern latitudes (Forkel et al., 2016; Graven et al., 2013). However, for autumn, even though ending of the growing season has been delayed because of autumn warming (Barichivich et al., 2013), land carbon-uptake termination time is found to have advanced as well, due to enhanced autumn respiration (Piao et al., 2008), which ultimately reduced the annual net ecosystem carbon uptake (Hadden and Grelle, 2016; Ueyama et al., 2014). For TeNH, we also found a significant negative relationship between land carbon-uptake anomalies and temperature for Q3 using the CAMS inversion data, consistent with the enhanced respiration by autumn warming found in the aforementioned studies. For Q4, however, both inversions point to decreasing land carbon uptakes with increasing precipitation. This finding might be due to enhanced respiration resulting from higher soil moisture content, but further site-scale examination is needed to confirm this hypothesis.

For BoNH and TeNH, land carbon-uptake anomalies are closely coupled with NDVI anomalies for Q2 (positive correlation, albeit an insignificant one for TeNH Q2 using Jena04 data), but they are generally de-coupled for Q3 and Q4, except that for Q3 of BoNH the CAMS-based land carbon uptake shows positive correlation with NDVI. This suggests high NDVI in autumn might not necessarily relate to a high land carbon uptake. There are two reasons: first, NDVI is found to correlate well with leaf-level CO_2 uptake for deciduous forest for different seasons, but is largely indepen-

dent of leaf photosynthesis for evergreen forests (Gamon et al., 1995). Second, even though a higher NDVI is associated with larger photosynthetic capacity and a higher gross photosynthesis, autumn warming might increase ecosystem respiration more than photosynthesis, leaving a net carbon source effect. Furthermore, other studies have also pointed out that severe summer drought can negate the enhanced carbon uptake during warm springs (Angert et al., 2005; Wolf et al., 2016).

4.2 Seasonal land carbon-uptake transitions in the tropics and influences of El Niño and vegetation fire

The strong transition to an abnormal source in the tropics and extratropical Southern Hemisphere was paralleled by a marked decrease in precipitation and an increase in temperature in Q4, with the development of El Niño in Q2–Q3 (Figs. S4l, S5l, S10). Here El Niño development is indicated by the rise of the MEI and Oceanic Niño Index (ONI, http://www.cpc.ncep.noaa.gov/products/analysis_monitoring/ensostuff/ONI_change.shtml). This strong transition is consistent with the expected response of tropical and sub-tropical southern ecosystems during previous El Niño events (Ahlström et al., 2015; Cox et al., 2013; Poulter et al., 2014; Wang et al., 2013, 2014). The weak abnormal source in Q1 in TroSH is consistent with a low precipitation anomaly. While temperature anomalies are abnormally high in Q2 and Q3, accompanied by extremely negative precipitation anomalies, the extremely low carbon flux in Q4 is largely explained by temperature, because correlations between land carbon uptake and precipitation in Q4 are very weak (Figs. S4i–l, S5i–l). Vegetation greenness has a significant positive correlation with land carbon-uptake anomalies only for Q1 in the tropics, and for the rest of the three seasons the correlation is very weak (Fig. S7i–l).

Compared with the 1997–1998 El Niño, which had a slightly larger MEI value, the 2015 El Niño started much earlier, with positive MEI and ONI appearing during the first half of 2014. Since then and until Q3 and Q4 in 2015 when El Niño began to reach its peak, the tropics and Southern Hemisphere saw continuous higher-than-normal temperatures, with continually decreasing precipitation and accumulating deficit in soil water content (Fig. S10). From Q3 to Q4, a steep decline is further observed in both precipitation and soil moisture with stagnating high-temperature anomaly, which is probably a major cause of the strong shift towards a carbon source anomaly. The CAMS inversion shows a carbon source anomaly in Q4 of 2015 slightly smaller than that in Q3 of 1997, while the Jena04 inversion shows almost equal magnitudes of loss in land sink strength between these two extreme El Niño events. On the one hand, El Niño in late 2015 started early and built upon the cumulative effects of the drought since the beginning of the year; it thus came with larger negative anomaly in precipitation and soil water content than the 1997–1998 El Niño. This sequence of events might favour a stronger land carbon source. On the other hand, the fire emission anomaly in the tropics in 2015 was less than half of that in 1997 at the peak of El Niño (Fig. S10); this might have contributed to a smaller land carbon-source anomaly in 2015 than in 1997–1998.

El Niño events are usually associated with increased vegetation fires, which have a large impact on the global carbon cycle (van der Werf et al., 2004). Global fire emissions of carbon reached 3.0 and 2.9 Pg C in 1997 and 1998 according to the GFED4s data. These 2 years produced the largest source of fire-emitted carbon for the entire period 1997–2015. In comparison, global fire emissions in 2015 reached 2.3 Pg C, close to the 1997–2015 average (2.2 Pg C yr^{-1}) but $\sim 25\,\%$ lower than 1997–1998 – the difference mainly occurring in the southern tropics (0–23.5° S; Fig. S10). In particular, carbon emissions from deforestation and peat fires were 2 times lower in 2015 (0.6 Pg C) compared with 1997 (1.2 Pg C) (GFED4s data). Emissions from these fire types are more likely to be a net carbon source, because they cannot be compensated by vegetation regrowth within a short time. Fire emission data thus suggest a smaller contribution from fires to AGR in 2015 than 1997–1998.

There has been a long debate on whether tropical vegetation shows enhanced greenness as indicated by vegetation indices (i.e. NDVI and enhanced vegetation index or EVI) during dry seasons or drought periods in tropical forest (Bi et al., 2015; Huete et al., 2006; Morton et al., 2014; Saleska et al., 2007; Samanta et al., 2010; Xu et al., 2011), and whether there is an accompanying decrease in long-term vegetation productivity associated with droughts (Medlyn, 2011; Samanta et al., 2011; Zhao and Running, 2010). Some studies show enhanced green-up in Amazonian forest during dry seasons mainly due to the release of radiation control on vegetation activities (Bi et al., 2015; Huete et al., 2006; Myneni et al., 2007), while Morton et al. (2014) argued that if errors in satellite observation angle are corrected, no increase in EVI can be observed during dry seasons. Saleska et al. (2007) observed a greener response of Amazonian forest during a severe drought event, whereas Samanta et al. (2010) argued such observed green-up is an artefact of atmosphere-corrupted data and the properly processed satellite observations revealed browner Amazonian forest during the severe drought event. Subsequent studies by Bi et al. (2016) and Xu et al. (2011) confirm the satellite-observed negative impacts of the drought events.

While long-term forest plot data demonstrated a consistent negative effect of droughts on tropical carbon uptake mainly through enhanced tree mortality (Lewis et al., 2011; Phillips et al., 2009), short-term site observations failed to reveal an immediate reduction in forest net primary productivity (Doughty et al., 2015) during drought, or reported even increased gross photosynthesis or photosynthetic capacity when entering dry season (Huete et al., 2006; Wu et al., 2016). Further, a large mortality event for trees will cause a legacy source over several years rather than a rapid re-

lease of CO_2 to the atmosphere during the year when trees died. Therefore, it remains challenging to reconcile immediate carbon-uptake reduction on the occurrence of drought in tropical ecosystems as diagnosed from atmospheric inversions (Gatti et al., 2014) and the aforementioned findings from forest plot data. In dynamic global vegetation models (DGVMs), the interannual variations of simulated land carbon sink are dominated by those in net primary production (Wang et al., 2016), which contradicts the site-level observations by Doughty et al. (2015).

Both Wang et al. (2013) and Wang et al. (2014) found a higher correlation coefficient between interannual variability in tropical land carbon fluxes (as inferred from interannual variations in AGR) with that in temperature than in precipitation, which is confirmed by our analysis of inversion-based tropical land carbon-flux anomalies with climate variations (Fig. 4). However, forest plot observations point to the prevailing drought as the dominant factor reducing forest carbon storage (Phillips et al., 2009). The need thus remains to reconcile the findings of temperature dominance on a large spatial scale and precipitation/moisture dominance on a fine scale. Recently, Jung et al. (2017) suggested that the dominant role of soil moisture over land carbon-flux anomalies shifts to temperature when the scale of spatial aggregation increases, due to the compensatory water effects in the process of spatial upscaling. We also find that for all seasons except Q3, inversion-based land carbon-uptake anomalies in the tropics and southern extratropics are positively correlated with soil water content (data not shown), with 2015 having an extremely low soil water content anomaly in Q4, echoing the extreme high-temperature anomaly shown in Fig. S4l. This might indicate that temperature impacts the land carbon uptake mainly by increasing evaporative demand and decreasing soil water content.

4.3 Data uncertainties and perspective

On the global and hemispheric scales, the inversion-derived land– and ocean–atmosphere fluxes are well constrained by the observed atmospheric CO_2 growth rates at measurement sites. However, because the observational network is heterogeneous and sites are sparsely distributed (Fig. S11), land CO_2 fluxes cannot be resolved precisely over each grid cell (Kaminski et al., 2001) and some regions are better constrained than others. This could hinder the precise pixel-scale matching between gridded CO_2 flux maps and climate states or the occurrence of climate extremes to investigate how climate extremes have affected carbon fluxes. Although we have identified that carbon-uptake transitions for some regions and seasons might be related to certain climate extremes (e.g. the role of precipitation in TeNH of Q4 shown in Fig. S5h), in general, exact attribution of these transitions into different climate drivers could be elusive. Further, a few other uncertainties matter for the specific objective of this study. First, the atmospheric network increased over time, so that the inversions have a better ability to detect and quantify a sharp transition in CO_2 fluxes occurring in the last than in the first decade of the period analysed. This might hide the detection of other more extreme end-of-year carbon transitions during the early years of our target period (1981–2015). Second, because measurements for early 2016 are not used in the CAMS inversion and are not completely available in the Jena04 inversion, the constraining of the last season in 2015 is weaker than for the other three seasons. This could influence estimating the exact magnitude of the extreme Q4 negative anomaly in land carbon uptake in 2015. Third, the sparse network of sites in boreal Eurasia and the tropics might diminish the ability of inversion systems to robustly allocate carbon fluxes spatially, which could yield high uncertainty in the carbon fluxes diagnosed for these regions (van der Laan-Luijkx et al., 2015; Stephens et al., 2007).

Despite these uncertainties, the strong transition of CO_2 fluxes from Q3 to Q4 is the largest ever found in the inversion records analysed here. Although 2015 shows extreme greening in the Northern Hemisphere, this strong greenness has been only translated into a moderate annual carbon sink anomaly in 2015, because vegetation greenness and land uptake anomalies are largely decoupled outside the growing season. The strong transition to a carbon source in TeNH in Q4 is consistent with the high precipitation that might have led to a large increase in respiration loss.

In the tropics, the transition to a strong source in TroSH in Q4 is congruent with the expected response of ecosystems to the peak of an El Niño event. However, given the ambiguous findings regarding changes in vegetation greenness during dry seasons or drought periods by previous studies (Saleska et al., 2007; Xu et al., 2011), and the uncertain roles of climate variations in driving the regional land carbon balance, more work is needed to reveal how these processes have evolved during opposing ENSO phases (i.e. the cold phase of La Niña versus the warm phase of El Niño). Furthermore, large-scale spatial observation-based analysis is hampered by the scarcity of sites measuring atmospheric concentrations or land–atmosphere fluxes with the eddy covariance method (Tramontana et al., 2016). For the BoTeNH, further investigation is still needed to verify whether a coupling between strong spring/summer uptake and autumn release is something intrinsic to natural ecosystems, or if strong transitions to autumn release are triggered by some particular extreme climate shifts. More detailed mechanisms can be explored by using long-term simultaneous observations of vegetation greenness and eddy covariance measurements of land–atmosphere fluxes combined with dynamic vegetation models. Here, our results point to the need to better understand the drivers of carbon dynamics on seasonal or even shorter timescales on the regional to global level, especially the link between such dynamics and climate extremes. Such understanding would help us make better predictions of the response of the carbon cycle to multiple long-term drivers such as atmospheric CO_2 growth and climate change.

5 Conclusions

We investigated the links among vegetation greenness, interannual land carbon flux variations and climate variations for 1981–2015 using inversion-based land carbon flux data sets. Consistent positive correlations between satellite-derived vegetation greenness and land carbon uptakes are found for the Northern Hemisphere during the growing season, but outside the growing season vegetation greenness and land carbon uptake are largely decoupled. Carbon uptake in the BoNH (> 45° N) is more consistently associated with temperature than precipitation, although such a pattern is less evident for the TeNH (23.5–45° N). Consistent with previous studies, we found a strong negative impact by temperature in the land carbon uptakes in the tropics and Southern Hemisphere, probably driven by the role of temperature in soil water content that tends to induce drought conditions.

We put an emphasis on the seasonal dynamics of land carbon uptake in 2015. We found that northern lands started with a higher-than-normal sink for the northern growing season, consistent with enhanced vegetation greenness partly owing to elevated warming. However, this enhanced sink was in part balanced by the carbon release in the autumn and winter, associated with extremely high precipitation in Q4 in the TeNH (23.5–45° N). Our results emphasized the important role of the coupling between seasonal carbon dynamics in the annual net carbon balance of the land ecosystem. More research is needed on whether such a coupling, between enhanced spring and summer sink and reduced autumn uptake, is something intrinsic in northern ecosystems, and on the frequency and extent of its occurrence. The dominance of temperature in the BoNH (> 45° N) and soil moisture in the TeNH (23–45° N) in their autumn carbon loss implies that future autumn temperature and precipitation change could have important consequences for the annual carbon balance of these regions. Hence, although continuing vegetation greening is projected mainly thanks to CO_2 fertilization (Zhu et al., 2016), such greening might not translate into enhanced land carbon uptake.

For the tropics and Southern Hemisphere, a strong transition was found towards a large carbon source for the last quarter of 2015, concomitant with the peak of El Niño development. This strong transition of terrestrial CO_2 fluxes in the last season is the largest in the inversion records since 1981, even though annual fire emissions were ∼ 25 % lower than during El Niño of 1997–1998. However, site-scale studies on tropical forest growth so far focusing on drought impacts cannot provide an adequate explanation of such strong transitions. It is unclear how the individual fluxes (gross primary production, net primary production and heterotrophic respiration) that make up the land carbon sink have responded to drought conditions. Our results point to the possibility that, with more frequent extreme El Niño events being projected in the future, such strong seasonal transitions in land carbon uptake might become more frequent and they can have substantial impact on the capacity of land ecosystems to sequester carbon.

Data availability. All data sets used in this study are available from the authors upon request.

The Supplement related to this article is available online at https://doi.org/10.5194/acp-17-13903-2017-supplement.

Author contributions. PC, FC, CY and AB conceived the study. CY performed the analysis and made the first draft. FC and CR provided the inversion data. TP provided the NDVI data. All authors contributed to the interpretation of the results and writing of the paper.

Competing interests. The authors declare that they have no conflict of interest.

Acknowledgements. Chao Yue and Philippe Ciais acknowledge funding from the European Commission's 7th Framework Programme, under grant agreement number 603542 (LUC4C). The work of Frederic Chevallier was funded by the Copernicus Atmosphere Monitoring Service, implemented by the European Centre for Medium-Range Weather Forecasts (ECMWF) on behalf of the European Commission. Taejin Park was supported by the NASA Earth and Space Science Fellowship Program (grant no. NNX16AO34H). We thank all the scientists involved in the surface and aircraft measurement of atmospheric CO_2 concentration and in archiving these data and making them available. We also thank the anonymous reviewers for their comments that helped improve the quality of the manuscript. We thank John Gash for improving the English of our manuscript.

Edited by: Silvia Kloster
Reviewed by: two anonymous referees

References

Adler, R. F., Huffman, G. J., Chang, A., Ferraro, R., Xie, P.-P., Janowiak, J., Rudolf, B., Schneider, U., Curtis, S., Bolvin, D., Gruber, A., Susskind, J., Arkin, P., and Nelkin, E.: The Version-2 Global Precipitation Climatology Project (GPCP) Monthly Precipitation Analysis (1979–Present), J. Hydrometeorol., 4, 1147–1167, https://doi.org/10.1175/1525-7541(2003)004<1147:TVGPCP>2.0.CO;2, 2003.

Ahlström, A., Raupach, M. R., Schurgers, G., Smith, B., Arneth, A., Jung, M., Reichstein, M., Canadell, J. G., Friedlingstein, P., Jain, A. K., Kato, E., Poulter, B., Sitch, S., Stocker, B. D., Viovy, N., Wang, Y. P., Wiltshire, A., Zaehle, S., and Zeng, N.: The dominant role of semi-arid ecosystems in the trend and variability of the land CO_2 sink, Science, 348, 895–899, https://doi.org/10.1126/science.aaa1668, 2015.

Angert, A., Biraud, S., Bonfils, C., Henning, C. C., Buermann, W., Pinzon, J., Tucker, C. J., and Fung, I.: Drier summers cancel out the CO_2 uptake enhancement induced by warmer springs, Proc. Natl. Acad. Sci. USA, 102, 10823–10827, https://doi.org/10.1073/pnas.0501647102, 2005.

Ballantyne, A. P., Alden, C. B., Miller, J. B., Tans, P. P., and White, J. W. C.: Increase in observed net carbon dioxide uptake by land and oceans during the past 50 years, Nature, 488, 70–72, https://doi.org/10.1038/nature11299, 2012.

Barichivich, J., Briffa, K. R., Myneni, R. B., Osborn, T. J., Melvin, T. M., Ciais, P., Piao, S., and Tucker, C.: Large-scale variations in the vegetation growing season and annual cycle of atmospheric CO_2 at high northern latitudes from 1950 to 2011, Glob. Change Biol., 19, 3167–3183, https://doi.org/10.1111/gcb.12283, 2013.

Bastos, A., Ciais, P., Park, T., Zscheischler, J., Yue, C., Barichivich, J., Myneni, R. B., Peng, S., Piao, S., and Zhu, Z.: Was the extreme Northern Hemisphere greening in 2015 predictable?, Environ. Res. Lett., 12, 044016, https://doi.org/10.1088/1748-9326/aa67b5, 2017.

Bi, J., Knyazikhin, Y., Choi, S., Park, T., Barichivich, J., Ciais, P., Fu, R., Sangram Ganguly, Hall, F., Hilker, T., Huete, A., Jones, M., Kimball, J., Lyapustin, A. I., Matti Mõttus, Nemani, R. R., Piao, S., Poulter, B., Saleska, S. R., Saatchi, S. S., Liang Xu, Zhou, L., and Myneni, R. B.: Sunlight mediated seasonality in canopy structure and photosynthetic activity of Amazonian rainforests, Environ. Res. Lett., 10, 064014, https://doi.org/10.1088/1748-9326/10/6/064014, 2015.

Bi, J., Myneni, R., Lyapustin, A., Wang, Y., Park, T., Chi, C., Yan, K., and Knyazikhin, Y.: Amazon forests' response to droughts: A perspective from the MAIAC product, Remote Sens., 8(4), 1–12, https://doi.org/10.3390/rs8040356, 2016.

Cai, W., Borlace, S., Lengaigne, M., van Rensch, P., Collins, M., Vecchi, G., Timmermann, A., Santoso, A., McPhaden, M. J., Wu, L., England, M. H., Wang, G., Guilyardi, E., and Jin, F.-F.: Increasing frequency of extreme El Niño events due to greenhouse warming, Nature Climate Change, 4, 111–116, https://doi.org/10.1038/nclimate2100, 2014.

Canadell, J. G., Le Quéré, C., Raupach, M. R., Field, C. B., Buitenhuis, E. T., Ciais, P., Conway, T. J., Gillett, N. P., Houghton, R. A., and Marland, G.: Contributions to accelerating atmospheric CO_2 growth from economic activity, carbon intensity, and efficiency of natural sinks, Proc. Natl. Acad. Sci. USA, 104, 18866–18870, 2007.

Chen, J., Jönsson, P., Tamura, M., Gu, Z., Matsushita, B., and Eklundh, L.: A simple method for reconstructing a high-quality NDVI time-series data set based on the Savitzky–Golay filter, Remote Sens. Environ., 91, 332–344, https://doi.org/10.1016/j.rse.2004.03.014, 2004.

Chevallier, F., Fisher, M., Peylin, P., Serrar, S., Bousquet, P., Bréon, F.-M., Chédin, A., and Ciais, P.: Inferring CO_2 sources and sinks from satellite observations: Method and application to TOVS data, J. Geophys. Res.-Atmos., 110, D24309, https://doi.org/10.1029/2005JD006390, 2005.

Chevallier, F., Ciais, P., Conway, T. J., Aalto, T., Anderson, B. E., Bousquet, P., Brunke, E. G., Ciattaglia, L., Esaki, Y., Fröhlich, M., Gomez, A., Gomez-Pelaez, A. J., Haszpra, L., Krummel, P. B., Langenfelds, R. L., Leuenberger, M., Machida, T., Maignan, F., Matsueda, H., Morguí, J. A., Mukai, H., Nakazawa, T., Peylin, P., Ramonet, M., Rivier, L., Sawa, Y., Schmidt, M., Steele, L. P., Vay, S. A., Vermeulen, A. T., Wofsy, S., and Worthy, D.: CO_2 surface fluxes at grid point scale estimated from a global 21 year reanalysis of atmospheric measurements, J. Geophys. Res.-Atmos., 115, D21307, https://doi.org/10.1029/2010JD013887, 2010.

Cox, P. M., Pearson, D., Booth, B. B., Friedlingstein, P., Huntingford, C., Jones, C. D., and Luke, C. M.: Sensitivity of tropical carbon to climate change constrained by carbon dioxide variability, Nature, 494, 341–344, https://doi.org/10.1038/nature11882, 2013.

Dee, D. P., Uppala, S. M., Simmons, A. J., Berrisford, P., Poli, P., Kobayashi, S., Andrae, U., Balmaseda, M. A., Balsamo, G., Bauer, P., Bechtold, P., Beljaars, A. C. M., van de Berg, L., Bidlot, J., Bormann, N., Delsol, C., Dragani, R., Fuentes, M., Geer, A. J., Haimberger, L., Healy, S. B., Hersbach, H., Hólm, E. V., Isaksen, L., Kållberg, P., Köhler, M., Matricardi, M., McNally, A. P., Monge-Sanz, B. M., Morcrette, J.-J., Park, B.-K., Peubey, C., de Rosnay, P., Tavolato, C., Thépaut, J.-N., and Vitart, F.: The ERA-Interim reanalysis: configuration and performance of the data assimilation system, Q. J. Roy. Meteor. Soc., 137, 553–597, https://doi.org/10.1002/qj.828, 2011.

Didan, K: MOD13C1 MODIS/Terra Vegetation Indices 16-Day L3 Global 0.05Deg CMG V006 NASA EOSDIS Land Processes DAAC, https://doi.org/10.5067/MODIS/MOD13C1.006, 2015.

Doughty, C. E., Metcalfe, D. B., Girardin, C. a. J., Amézquita, F. F., Cabrera, D. G., Huasco, W. H., Silva-Espejo, J. E., Araujo-Murakami, A., da Costa, M. C., Rocha, W., Feldpausch, T. R., Mendoza, A. L. M., da Costa, A. C. L., Meir, P., Phillips, O. L., and Malhi, Y.: Drought impact on forest carbon dynamics and fluxes in Amazonia, Nature, 519, 78–82, https://doi.org/10.1038/nature14213, 2015.

Field, R. D., Werf, G. R. van der, Fanin, T., Fetzer, E. J., Fuller, R., Jethva, H., Levy, R., Livesey, N. J., Luo, M., Torres, O., and Worden, H. M.: Indonesian fire activity and smoke pollution in 2015 show persistent nonlinear sensitivity to El Niño-induced drought, Proc. Natl. Acad. Sci. USA, 113, 9204–9209, https://doi.org/10.1073/pnas.1524888113, 2016.

Forkel, M., Carvalhais, N., Rödenbeck, C., Keeling, R., Heimann, M., Thonicke, K., Zaehle, S., and Reichstein, M.: Enhanced seasonal CO_2 exchange caused by amplified plant productivity in northern ecosystems, Science, 351, 696–699, https://doi.org/10.1126/science.aac4971, 2016.

Gamon, J. A., Field, C. B., Goulden, M. L., Griffin, K. L., Hartley, A. E., Joel, G., Peñuelas, J., and Valentini, R.: Relationships Between NDVI, Canopy Structure, and Photosynthesis in Three Californian Vegetation Types, Ecol. Appl., 5, 28–41, https://doi.org/10.2307/1942049, 1995.

Gatti, L. V., Gloor, M., Miller, J. B., Doughty, C. E., Malhi, Y., Domingues, L. G., Basso, L. S., Martinewski, A., Correia, C. S. C., Borges, V. F., Freitas, S., Braz, R., Anderson, L. O., Rocha, H., Grace, J., Phillips, O. L., and Lloyd, J.: Drought sensitivity of Amazonian carbon balance revealed by atmospheric measurements, Nature, 506, 76–80, https://doi.org/10.1038/nature12957, 2014.

Graven, H. D., Keeling, R. F., Piper, S. C., Patra, P. K., Stephens, B. B., Wofsy, S. C., Welp, L. R., Sweeney, C., Tans, P. P., Kelley, J. J., Daube, B. C., Kort, E. A., Santoni, G. W., and Bent, J. D.: Enhanced Seasonal Exchange of CO_2 by Northern Ecosystems Since 1960, Science, 341, 1085–1089, https://doi.org/10.1126/science.1239207, 2013.

Gu, L., Baldocchi, D. D., Wofsy, S. C., Munger, J. W., Michalsky, J. J., Urbanski, S. P., and Boden, T. A.: Response of a Deciduous Forest to the Mount Pinatubo Eruption: Enhanced Photosynthesis, Science, 299, 2035–2038, https://doi.org/10.1126/science.1078366, 2003.

Hadden, D. and Grelle, A.: Changing temperature response of respiration turns boreal forest from carbon sink into carbon source, Agr. Forest Meteorol., 223, 30–38, https://doi.org/10.1016/j.agrformet.2016.03.020, 2016.

Huete, A. R., Didan, K., Shimabukuro, Y. E., Ratana, P., Saleska, S. R., Hutyra, L. R., Yang, W., Nemani, R. R., and Myneni, R.: Amazon rainforests green-up with sunlight in dry season, Geophys. Res. Lett., 33, L06405, https://doi.org/10.1029/2005GL025583, 2006.

Huijnen, V., Wooster, M. J., Kaiser, J. W., Gaveau, D. L. A., Flemming, J., Parrington, M., Inness, A., Murdiyarso, D., Main, B., and van Weele, M.: Fire carbon emissions over maritime southeast Asia in 2015 largest since 1997, Sci. Rep., 6, 26886, https://doi.org/10.1038/srep26886, 2016.

Jacobson, A. R., Mikaloff Fletcher, S. E., Gruber, N., Sarmiento, J. L., and Gloor, M.: A joint atmosphere-ocean inversion for surface fluxes of carbon dioxide: 1. Methods and global-scale fluxes, Global Biogeochem. Cy., 21, GB1019, https://doi.org/10.1029/2005GB002556, 2007.

Jiménez-Muñoz, J. C., Mattar, C., Barichivich, J., Santamaría-Artigas, A., Takahashi, K., Malhi, Y., Sobrino, J. A., and van der Schrier, G.: Record-breaking warming and extreme drought in the Amazon rainforest during the course of El Niño 2015–2016, Sci. Rep., 6, 33130, https://doi.org/10.1038/srep33130, 2016.

Jönsson, P. and Eklundh, L.: TIMESAT – a program for analyzing time-series of satellite sensor data, Comput. Geosci., 30, 833–845, https://doi.org/10.1016/j.cageo.2004.05.006, 2004.

Jung, M., Reichstein, M., Schwalm, C. R., Huntingford, C., Sitch, S., Ahlström, A., Arneth, A., Camps-Valls, G., Ciais, P., Friedlingstein, P., Gans, F., Ichii, K., Jain, A. K., Kato, E., Papale, D., Poulter, B., Raduly, B., Rödenbeck, C., Tramontana, G., Viovy, N., Wang, Y.-P., Weber, U., Zaehle, S., and Zeng, N.: Compensatory water effects link yearly global land CO_2 sink changes to temperature, Nature, 541, 7638, https://doi.org/10.1038/nature20780, 2017.

Kaminski, T., Rayner, P. J., Heimann, M., and Enting, I. G.: On aggregation errors in atmospheric transport inversions, J. Geophys. Res.-Atmos., 106, 4703–4715, https://doi.org/10.1029/2000JD900581, 2001.

Le Quéré, C. L., Andrew, R. M., Canadell, J. G., Sitch, S., Korsbakken, J. I., Peters, G. P., Manning, A. C., Boden, T. A., Tans, P. P., Houghton, R. A., Keeling, R. F., Alin, S., Andrews, O. D., Anthoni, P., Barbero, L., Bopp, L., Chevallier, F., Chini, L. P., Ciais, P., Currie, K., Delire, C., Doney, S. C., Friedlingstein, P., Gkritzalis, T., Harris, I., Hauck, J., Haverd, V., Hoppema, M., Klein Goldewijk, K., Jain, A. K., Kato, E., Körtzinger, A., Landschützer, P., Lefèvre, N., Lenton, A., Lienert, S., Lombardozzi, D., Melton, J. R., Metzl, N., Millero, F., Monteiro, P. M. S., Munro, D. R., Nabel, J. E. M. S., Nakaoka, S., O'Brien, K., Olsen, A., Omar, A. M., Ono, T., Pierrot, D., Poulter, B., Rödenbeck, C., Salisbury, J., Schuster, U., Schwinger, J., Séférian, R., Skjelvan, I., Stocker, B. D., Sutton, A. J., Takahashi, T., Tian, H., Tilbrook, B., Laan-Luijkx, I. T. van der, Werf, G. R. van der, Viovy, N., Walker, A. P., Wiltshire, A. J., and Zaehle, S.: Global Carbon Budget 2016, Earth Syst. Sci. Data, 8, 605–649, https://doi.org/10.5194/essd-8-605-2016, 2016.

Lewis, S. L., Brando, P. M., Phillips, O. L., van der Heijden, G. M., and Nepstad, D.: The 2010 amazon drought, Science, 331, 554–554, 2011.

Li, W., Ciais, P., Wang, Y., Peng, S., Broquet, G., Ballantyne, A. P., Canadell, J. G., Cooper, L., Friedlingstein, P., Quéré, C. L., Myneni, R. B., Peters, G. P., Piao, S., and Pongratz, J.: Reducing uncertainties in decadal variability of the global carbon budget with multiple datasets, Proc. Natl. Acad. Sci. USA, 113, 13104–13108, https://doi.org/10.1073/pnas.1603956113, 2016.

Medlyn, B. E.: Comment on "Drought-Induced Reduction in Global Terrestrial Net Primary Production from 2000 Through 2009", Science, 333, 1093–1093, https://doi.org/10.1126/science.1199544, 2011.

Morton, D. C., Nagol, J., Carabajal, C. C., Rosette, J., Palace, M., Cook, B. D., Vermote, E. F., Harding, D. J., and North, P. R. J.: Amazon forests maintain consistent canopy structure and greenness during the dry season, Nature, 506, 221–224, https://doi.org/10.1038/nature13006, 2014.

Myneni, R. B., Keeling, C. D., Tucker, C. J., Asrar, G., and Nemani, R. R.: Increased plant growth in the northern high latitudes from 1981 to 1991, Nature, 386, 698–702, https://doi.org/10.1038/386698a0, 1997.

Myneni, R. B., Yang, W., Nemani, R. R., Huete, A. R., Dickinson, R. E., Knyazikhin, Y., Didan, K., Fu, R., Juárez, R. I. N., Saatchi, S. S., Hashimoto, H., Ichii, K., Shabanov, N. V., Tan, B., Ratana, P., Privette, J. L., Morisette, J. T., Vermote, E. F., Roy, D. P., Wolfe, R. E., Friedl, M. A., Running, S. W., Votava, P., El-Saleous, N., Devadiga, S., Su, Y., and Salomonson, V. V.: Large seasonal swings in leaf area of Amazon rainforests, Proc. Natl. Acad. Sci. USA, 104, 4820–4823, https://doi.org/10.1073/pnas.0611338104, 2007.

Nemani, R. R., Keeling, C. D., Hashimoto, H., Jolly, W. M., Piper, S. C., Tucker, C. J., Myneni, R. B., and Running, S. W.: Climate-Driven Increases in Global Terrestrial Net Primary Production from 1982 to 1999, Science, 300, 1560–1563, https://doi.org/10.1126/science.1082750, 2003.

Orth, R., Zscheischler, J., and Seneviratne, S. I.: Record dry summer in 2015 challenges precipitation projections in Central Europe, Sci. Rep., 6, 28334, https://doi.org/10.1038/srep28334, 2016.

Phillips, O. L., Aragão, L. E. O. C., Lewis, S. L., Fisher, J. B., Lloyd, J., López-González, G., Malhi, Y., Monteagudo, A., Peacock, J., Quesada, C. A., Heijden, G. van der, Almeida, S., Amaral, I., Arroyo, L., Aymard, G., Baker, T. R., Bánki, O., Blanc, L., Bonal, D., Brando, P., Chave, J., Oliveira, Á. C. A. de, Cardozo, N. D., Czimczik, C. I., Feldpausch, T. R., Freitas, M. A., Gloor, E., Higuchi, N., Jiménez, E., Lloyd, G., Meir, P., Mendoza, C., Morel, A., Neill, D. A., Nepstad, D., Patiño, S., Peñuela, M. C., Prieto, A., Ramírez, F., Schwarz, M., Silva, J., Silveira, M., Thomas, A. S., Steege, H. ter, Stropp, J., Vásquez, R., Zelazowski, P., Dávila, E. A., Andelman, S., Andrade, A., Chao, K.-J., Erwin, T., Fiore, A. D., C, E. H., Keeling, H., Killeen, T. J., Laurance, W. F., Cruz, A. P., Pitman, N. C. A., Vargas, P. N., Ramírez-Angulo, H., Rudas, A., Salamão, R., Silva, N., Terborgh, J., and Torres-Lezama, A.: Drought Sensitivity of the Amazon Rainforest, Science, 323, 1344–1347, https://doi.org/10.1126/science.1164033, 2009.

Piao, S., Ciais, P., Friedlingstein, P., Peylin, P., Reichstein, M., Luyssaert, S., Margolis, H., Fang, J., Barr, A., Chen, A., Grelle, A., Hollinger, D. Y., Laurila, T., Lindroth, A., Richardson, A. D., and Vesala, T.: Net carbon dioxide losses of northern ecosystems in response to autumn warming, Nature, 451, 49–52, https://doi.org/10.1038/nature06444, 2008.

Poulter, B., Frank, D., Ciais, P., Myneni, R. B., Andela, N., Bi, J., Broquet, G., Canadell, J. G., Chevallier, F., Liu, Y. Y., Running, S. W., Sitch, S., and van der Werf, G. R.: Contribution of semi-arid ecosystems to interannual variability of the global carbon cycle, Nature, 509, 600–603, https://doi.org/10.1038/nature13376, 2014.

Prather, M. J., Holmes, C. D., and Hsu, J.: Reactive greenhouse gas scenarios: Systematic exploration of uncertainties and the role of atmospheric chemistry, Geophys. Res. Lett., 39, L09803, https://doi.org/10.1029/2012GL051440, 2012.

Rödenbeck, C.: Estimating CO_2 sources and sinks from atmospheric mixing ratio measurements using a global inversion of atmospheric transport, Max Planck Institute for Biogeochemistry, 2005.

Rödenbeck, C., Houweling, S., Gloor, M., and Heimann, M.: CO_2 flux history 1982–2001 inferred from atmospheric data using a global inversion of atmospheric transport, Atmos. Chem. Phys., 3, 1919–1964, https://doi.org/10.5194/acp-3-1919-2003, 2003.

Saleska, S. R., Didan, K., Huete, A. R., and da Rocha, H. R.: Amazon Forests Green-Up During 2005 Drought, Science, 318, 612–612, https://doi.org/10.1126/science.1146663, 2007.

Samanta, A., Ganguly, S., Hashimoto, H., Devadiga, S., Vermote, E., Knyazikhin, Y., Nemani, R. R., and Myneni, R. B.: Amazon forests did not green-up during the 2005 drought, Geophys. Res. Lett., 37, L05401, https://doi.org/10.1029/2009GL042154, 2010.

Samanta, A., Costa, M. H., Nunes, E. L., Vieira, S. A., Xu, L., and Myneni, R. B.: Comment on "Drought-Induced Reduction in Global Terrestrial Net Primary Production from 2000 Through 2009", Science, 333, 1093–1093, https://doi.org/10.1126/science.1199048, 2011.

Savitzky, A. and Golay, M. J. E.: Smoothing and Differentiation of Data by Simplified Least Squares Procedures, Anal. Chem., 36, 1627–1639, https://doi.org/10.1021/ac60214a047, 1964.

Stephens, B. B., Gurney, K. R., Tans, P. P., Sweeney, C., Peters, W., Bruhwiler, L., Ciais, P., Ramonet, M., Bousquet, P., Nakazawa, T., Aoki, S., Machida, T., Inoue, G., Vinnichenko, N., Lloyd, J., Jordan, A., Heimann, M., Shibistova, O., Langenfelds, R. L., Steele, L. P., Francey, R. J., and Denning, A. S.: Weak Northern and Strong Tropical Land Carbon Uptake from Vertical Profiles of Atmospheric CO_2, Science, 316, 1732–1735, https://doi.org/10.1126/science.1137004, 2007.

Tanja, S., Berninger, F., Vesala, T., Markkanen, T., Hari, P., Mäkelä, A., Ilvesniemi, H., Hänninen, H., Nikinmaa, E., Huttula, T., Laurila, T., Aurela, M., Grelle, A., Lindroth, A., Arneth, A., Shibistova, O., and Lloyd, J.: Air temperature triggers the recovery of evergreen boreal forest photosynthesis in spring, Glob. Change Biol., 9, 1410–1426, https://doi.org/10.1046/j.1365-2486.2003.00597.x, 2003.

Tramontana, G., Jung, M., Schwalm, C. R., Ichii, K., Camps-Valls, G., Ráduly, B., Reichstein, M., Arain, M. A., Cescatti, A., Kiely, G., Merbold, L., Serrano-Ortiz, P., Sickert, S., Wolf, S., and Papale, D.: Predicting carbon dioxide and energy fluxes across global FLUXNET sites with regression algorithms, Biogeosciences, 13, 4291–4313, https://doi.org/10.5194/bg-13-4291-2016, 2016.

Ueyama, M., Iwata, H., and Harazono, Y.: Autumn warming reduces the CO_2 sink of a black spruce forest in interior Alaska based on a nine-year eddy covariance measurement, Glob. Change Biol., 20, 1161–1173, https://doi.org/10.1111/gcb.12434, 2014.

Wang, J., Zeng, N., and Wang, M.: Interannual variability of the atmospheric CO_2 growth rate: roles of precipitation and temperature, Biogeosciences, 13, 2339–2352, https://doi.org/10.5194/bg-13-2339-2016, 2016.

Wang, W., Ciais, P., Nemani, R. R., Canadell, J. G., Piao, S., Sitch, S., White, M. A., Hashimoto, H., Milesi, C., and Myneni, R. B.: Variations in atmospheric CO_2 growth rates coupled with tropical temperature, Proc. Natl. Acad. Sci. USA, 110, 13061–13066, https://doi.org/10.1073/pnas.1219683110, 2013.

Wang, X., Piao, S., Ciais, P., Friedlingstein, P., Myneni, R. B., Cox, P., Heimann, M., Miller, J., Peng, S., Wang, T., Yang, H., and Chen, A.: A two-fold increase of carbon cycle sensitivity to tropical temperature variations, Nature, 506, 212–215, https://doi.org/10.1038/nature12915, 2014.

van der Laan-Luijkx, I. T., van der Velde, I. R., Krol, M. C., Gatti, L. V., Domingues, L. G., Correia, C. S. C., Miller, J. B., Gloor, M., van Leeuwen, T. T., Kaiser, J. W., Wiedinmyer, C., Basu, S., Clerbaux, C., and Peters, W.: Response of the Amazon carbon balance to the 2010 drought derived with CarbonTracker South America, Global Biogeochem. Cy., 29, GB005082, https://doi.org/10.1002/2014GB005082, 2015.

van der Werf, G. R., Randerson, J. T., Collatz, G. J., Giglio, L., Kasibhatla, P. S., Arellano, A. F., Olsen, S. C., and Kasischke, E. S.: Continental-Scale Partitioning of Fire Emissions During the 1997 to 2001 El Niño/La Niña Period, Science, 303, 73–76, https://doi.org/10.1126/science.1090753, 2004.

van der Werf, G. R., Dempewolf, J., Trigg, S. N., Randerson, J. T., Kasibhatla, P. S., Giglio, L., Murdiyarso, D., Peters, W., Morton, D. C., Collatz, G. J., Dolman, A. J., and DeFries, R. S.: Climate regulation of fire emissions and deforestation in equatorial Asia, Proc. Natl. Acad. Sci. USA, 105, 20350–20355, https://doi.org/10.1073/pnas.0803375105, 2008.

Wolf, S., Keenan, T. F., Fisher, J. B., Baldocchi, D. D., Desai, A. R., Richardson, A. D., Scott, R. L., Law, B. E., Litvak, M. E., Brunsell, N. A., Peters, W., and Laan-Luijkx, I. T. van der: Warm spring reduced carbon cycle impact of the 2012 US summer drought, Proc. Natl. Acad. Sci. USA, 113, 5880–5885, https://doi.org/10.1073/pnas.1519620113, 2016.

Wolter, K. and Timlin, M. S.: El Niño/Southern Oscillation behaviour since 1871 as diagnosed in an extended multivariate ENSO index (MEI.ext), Int. J. Climatol., 31, 1074–1087, https://doi.org/10.1002/joc.2336, 2011.

Wu, J., Albert, L. P., Lopes, A. P., Restrepo-Coupe, N., Hayek, M., Wiedemann, K. T., Guan, K., Stark, S. C., Christoffersen, B., Prohaska, N., Tavares, J. V., Marostica, S., Kobayashi, H., Ferreira, M. L., Campos, K. S., Silva, R. da, Brando, P. M., Dye, D. G., Huxman, T. E., Huete, A. R., Nelson, B. W., and Saleska, S. R.: Leaf development and demography explain photosynthetic seasonality in Amazon evergreen forests, Science, 351, 972–976, https://doi.org/10.1126/science.aad5068, 2016.

Xu, L., Samanta, A., Costa, M. H., Ganguly, S., Nemani, R. R., and Myneni, R. B.: Widespread decline in greenness of Amazo-

nian vegetation due to the 2010 drought, Geophys. Res. Lett., 38, L07402, https://doi.org/10.1029/2011GL046824, 2011.

Yin, Y., Ciais, P., Chevallier, F., van der Werf, G. R., Fanin, T., Broquet, G., Boesch, H., Cozic, A., Hauglustaine, D., Szopa, S., and Wang, Y.: Variability of fire carbon emissions in equatorial Asia and its nonlinear sensitivity to El Niño, Geophys. Res. Lett., 43, GL070971, https://doi.org/10.1002/2016GL070971, 2016.

Zhao, M. and Running, S. W.: Drought-Induced Reduction in Global Terrestrial Net Primary Production from 2000 Through 2009, Science, 329, 940–943, https://doi.org/10.1126/science.1192666, 2010.

Zhou, L., Tucker, C. J., Kaufmann, R. K., Slayback, D., Shabanov, N. V., and Myneni, R. B.: Variations in northern vegetation activity inferred from satellite data of vegetation index during 1981 to 1999, J. Geophys. Res.-Atmos, 106, 20069–20083, https://doi.org/10.1029/2000JD000115, 2001.

Zhu, Z., Piao, S., Myneni, R. B., Huang, M., Zeng, Z., Canadell, J. G., Ciais, P., Sitch, S., Friedlingstein, P., Arneth, A., Cao, C., Cheng, L., Kato, E., Koven, C., Li, Y., Lian, X., Liu, Y., Liu, R., Mao, J., Pan, Y., Peng, S., Peñuelas, J., Poulter, B., Pugh, T. A. M., Stocker, B. D., Viovy, N., Wang, X., Wang, Y., Xiao, Z., Yang, H., Zaehle, S., and Zeng, N.: Greening of the Earth and its drivers, Nature Climate Change, 6, 791–795, https://doi.org/10.1038/nclimate3004, 2016.